GSA DATA REPOSITORY 2017292

Uranium and carbon isotopes document global-ocean redox-productivity relationships linked to cooling during the Frasnian-Famennian boundary mass extinction

Huyue Song, Haijun Song, Thomas J. Algeo, Jinnan Tong, Stephen J. Romaniello, Yuanyuan Zhu, Daoliang Chu, Yiming Gong, and Ariel D. Anbar

(DR1) REGIONAL PALEOGEOGRAPHY AND STRATIGRAPHY

The Baisha section is located on the outer margin of the Guilin Platform of the Nanpanjiang Basin (Fig. DR1). Frasnian strata consist mainly of thin-bedded limestones with some interbeds of siltstone and banded chert belonging to the Liujiang Formation, whereas Famennian strata are mainly nodular limestones of the Wuzhishan Formation. The carbonates at Baisha are mainly of pelagic origin, representing open-marine sedimentation (Chen and Tucker, 2003; Chen et al., 2005).

A northeastward marine transgression of the South China Craton began in the Early Devonian and reached a highstand in the Frasnian (Chen and Tucker, 2003). In the early Givetian, the area of carbonate deposition expanded considerably, while siliciclastic sediments retreated to shorelines around landmasses. From the late Givetian to early Frasnian, the South China Craton was fragmented through transtensional and extensional tectonics into areas of small platforms and basins (Fig. DR1; Chen et al., 2001a, b). This event produced elongate platform-basin systems trending NNE-SSW from eastern Guangxi to central Hunan,

and an orthogonal platform system trending NW-SE and NE-SW in western Guangxi (Chen and Tucker, 2003). Subsequently, multiple marine transgressions and regressions are recorded through the F-F transition, leading to development of a number of distinct facies, including nearshore sandy, subtidal mixed carbonate-siliciclastic, inter-platform, open-platform, platform marginal, slope, and basinal facies (Ma et al., 2016).

Global conodont studies have established three conodont zones in the late Frasnian: the Lower *Palmatolepis rhenana*, Upper *Pa. rhenana*, and *Pa. linguiformis* zones (Ziegler and Sandberg, 1990; Ma et al., 2016). The Lower Famennian was previously subdivided into the Lower, Middle and Upper *Pa. triangularis* zones (Ziegler and Sandberg, 1990), but Spalletta et al. (2017) recently revised this as follows: (1) the Lower *triangularis* Zone has been subdivided into the *Pa. subperlobata* Zone and *Pa. triangularis* Zone; and (2) the Middle and Upper *triangularis* zones have been renamed the *Pa. delicatula platys* and *Pa. minuta minuta* zones, respectively. Regional conodont biostratigraphic data for central South China were reviewed in Ma et al. (2016), who followed the Ziegler and Sandberg (1990) zonation scheme. Herein, we update the zonation terminology to that of Spalletta et al (2017), while inserting a dashed line between the *subperlobata* and *triangularis* zones, which have not yet been separately discriminated in the study region.

Abundant pelagic and benthic faunas, including cephalopods, conodonts, ostracods, corals, brachiopods, and radiolarians, are recorded in F-F strata of South China. In this area, the LKH coincided with a massive loss of reef facies, and the UKH with a three-stage mass extinction among marine invertebrates (Ma et al., 2016, their figure 11): (1) MEBF-1 (mass

extinction of benthic fauna): disappearance of diverse deep-water brachiopods (including most atrypids), probably correlative with the base of the Upper Kellwasser Horizon of Sandberg et al. (2002); (2) CE-1 (conodont extinction): disappearance of conodonts in the middle part of the Upper Kellwasser; and (3) MEBF-2 and CE-2: the final demise of the diverse and abundant shallow-water rugose coral and ostracod faunas, at a level probably corresponding to the base of the 'Extinction Shale' of Sandberg et al. (2002). In the aftermath of the FFB mass extinction, recovery rates differed among biotic groups. *Palmatolepis* conodonts began to recover immediately after the FFB crisis, in the *Pa. subperlobata-triangularis* zones (= Lower *Pa. triangularis* Zone), whereas benthic ostracods, brachiopods, and radiolarians began to recover somewhat later, in the *Pa. delicatula platys* and *Pa. minuta minuta* zones (= Middle and Upper *Pa. triangularis* zones, respectively) (Ma et al., 2016). Recently, it has been argued that the main cause of biodiversity decline during the F-F transition was reduced speciation rates rather than elevated extinction rates (Alroy, 2008; Stigall, 2012), but this is not supported by faunal patterns in South China (Wang and Ziegler, 2002; Shen and Webb, 2004; Ma et al., 2016).

(DR2) ANALYTICAL METHODS

Fresh carbonate samples were collected from the Baisha section. Weathered surfaces and veins were trimmed off, and the remaining sample material was cut into small pieces and ground to a fine powder using a ball mill at Wuhan Institute of Geology and Mineral Resources. Total organic carbon (TOC) content was measured using an Eltra 2000 C-S

analyzer at the University of Cincinnati. Data quality was monitored via analysis of USGS standard SDO-1 (C = 9.68 %; S = 5.35 %) and an internal lab standard (DBS-1; C = 3.50 %; S = 1.97 %), which yielded an analytical precision (2σ) of ±2.5 % of reported values for TOC and ±5 % of reported values for S.

Carbon and oxygen isotopic compositions were measured using a Thermo Fisher Gasbench II-MAT 253 stable isotope mass spectrometer at the State Key Laboratory of Biogeology and Environmental Geology in the China University of Geosciences (Wuhan). About 150-400 μg of powder was placed in a 10 mL Na-glass vial, sealed with a butyl rubber septum, and reacted with 100 % phosphoric acid at 72 °C after flushing with helium using the Gasbench II interface. The $\delta^{13}C$ and $\delta^{18}O$ compositions of the evolved CO_2 gas were measured and reported as per mille variation relative to the Vienna Pee Dee Belemnite (VPDB) standard. Data quality was monitored via repeated analysis of two Chinese national standards, GBW 04416 ($\delta^{13}C$ = +1.61 ‰, $\delta^{18}O$ = –11.59 ‰) and GBW 04417 ($\delta^{13}C$ = –6.06 ‰, $\delta^{18}O$ = –24.12 ‰), which yielded analytical precisions (2σ) of better than ±0.1 ‰ for $\delta^{13}C$ and $\delta^{18}O$. In addition, one sample out of every ten was re-analyzed as a replicate, to check the precision of unknowns.

U concentrations and isotopes were measured at Arizona State University. About 3-4 g of sample powder were dissolved in 1 M HNO_3 for 24 h and centrifuged to separate the insoluble residues from the acid soluble solutes. The trace elemental concentrations of carbonates in the dissolved solution were analyzed using a Thermo ICPQ ICP-MS. The solution, containing ~500 ng U, was then spiked with an IRMM 3636 uranium double spike

to give a $^{233}U/^{235}U$ ratio of 2.5 and dried down to homogenize the spike-sample mixture. The sample was redissolved in 3 M HNO_3, and U was separated from the sample matrix using the UTEVE resin protocol described by Weyer et al. (2008), modified by extending the 3 M HNO_3 matrix elution step to 12 mL in order to completely remove the large amounts of calcium present in carbonate samples. After column chemistry, the sample was treated twice with a HNO_3/H_2O_2 mixture to remove residual organics from the resin and dissolved in 2 % HNO_3 for isotopic analysis. Uranium isotope measurements were performed on a ThermoFinnigan Neptune MC-ICP-MS instrument. The U isotopic compositions of the samples are reported as $\delta^{238}U$ ($^{238}U/^{235}U$) relative to the U isotope standard CRM-145. Internal precision (2σ) based on replicate measurements of standards was 0.08 ‰. Average reproducibility (2σ), assessed by replicate measurements of the same sample solution, was 0.11 ‰. We analyzed reference materials BCR-2 (Columbia River Basalt), CRM129a, and SRM950a to monitor reproducibility and check agreement with previously published values.

(DR3) DIAGENETIC INFLUENCES ON STUDY SAMPLES

Several studies have demonstrated that carbonate U isotopes can be altered by diagenesis or detrital inputs (Romaniello et al., 2013; Anderson et al., 2014; Tissot and Dauphas, 2015). Here, we investigated relationships between U elemental (i.e., Th/U) and isotopic (i.e., $\delta^{238}U$) compositions versus the $\delta^{18}O$, Mg/Ca, Sr/Ca, and Al content of the study samples to evaluate the robustness of our U-isotope dataset as a primary record.

Post-depositional solution-precipitation reactions in the host carbonate sediment can leach U from calcite, altering Th/U ratios (Chung and Swart, 1990). However, any potential U leaching would have affected U concentrations and not $\delta^{238}U$ values (given a lack of fractionation among U isotopes during weathering; Weyer et al., 2008). Of particular importance is that there is no evidence for meteoric diagenesis of the study succession, and the near-lack of organic matter throughout the section (TOC values mostly <0.2 %; Table DR1) offered limited potential for late-stage burial diagenesis through sulfate reduction or methanogenesis. Oxygen-isotope values are mostly –6 ‰ to –8 ‰, with limited sample-to-sample variation and only a weak long-term stratigraphic trend (Table DR1). Thus, the entire section appears to have experienced similar burial diagenetic conditions with no evidence for meteoric diagenesis.

Th is delivered to marine sediments in detrital siliciclastics (mainly clays), and it is relatively immobile in the diagenetic environment (Thomson et al., 1998). U can accumulate in marine sediments in several forms, including detrital, phosphate-bound, and organic-bound fractions (the latter two as authigenic/secondary phases; Cumberland et al., 2016). Given typical concentrations in shale/upper continental crust-derived sediments (10.7 ppm Th, 2.8 ppm U; McLennan, 2001), Th/U ratios should be ~4 in sediments without authigenic U enrichment. Wignall and Twitchett (1996) cited Th/U ratios of 2 to 7 for oxic facies versus Th/U ratios <2 for anoxic facies in which authigenic U enrichment is present. The degree of authigenic U enrichment depends on seawater U concentrations, however, and if widespread oceanic anoxia results in seawater U drawdown, then the authigenic U fraction of the

sediment will also decline (cf. Algeo, 2004). Following initial deposition, diagenesis can modify sediment Th/U ratios, mainly as a result of U remobilization given the relative immobility of Th (Thomson et al., 1998). U can readily adsorb/desorb from some phases (especially organics) due to redox changes in sediment porewaters (Cumberland et al., 2016). U in phosphate is structurally bound and less subject to secondary remobilization.

Diagenetic alteration of U-isotope signals is potentially a concern in carbonate sediments. For example, dolomitization can result in a decrease of $\delta^{238}U$ (Romaniello et al., 2013). All samples in this study yielded Mg/Ca ratios <0.1 (0.01-0.04; Table DR1), indicating that dolomitization is insignificant. Th/U content exhibits a positive correlation with Mg/Ca ratios ($r = +0.55$, $p < 0.01$; Fig. DR2A), but the significance of this relationship is unclear given the limited range and small values of Mg/Ca in the study samples. Th/U exhibits a moderate relationship to $\delta^{238}U$ ($r = -0.39$, $p < 0.05$; Fig. DR3A), which is in any case unsurprising if both variables were controlled by global-ocean redox conditions. $\delta^{13}C_{carb}$ exhibits no correlation with $\delta^{18}O$ ($r = +0.04$, $p >> 0.05$; Fig. DR4A) but a moderate correlation with TOC ($r = +0.39$, $p < 0.05$; Fig. DR4B). The latter relationship suggests some linkage between local marine productivity (proxied by TOC) and global marine productivity (proxied by $\delta^{13}C_{carb}$). Finally, Sr/Ca ratios show no correlation with Th/U ($r = -0.37$, $p > 0.05$; Fig. DR2B) or $\delta^{238}U$ ($r = -0.25$, $p > 0.05$; DR3B). These observations are consistent with well-preserved primary marine geochemical signatures at Baisha, and they provide no evidence of diagenetic alteration of the U-isotopic compositions of the study samples.

Detrital inputs are regarded as a main cause of post-depositional alteration of U-isotope signals (Asael et al., 2013; Andersen et al., 2014). In the study samples, we did not detect any relationship between Al content and $\delta^{238}U$ ($r = -0.27$, $p > 0.05$; Fig. DR3C). However, there is a distinct correlation between Al content and Th/U ratios ($r = +0.85$, $p < 0.001$; Fig. DR2C). This relationship appears to be an artifact of strong correlation between Th and Al contents ($r = +0.91$, $p < 0.001$; Fig. DR2D). However, Al concentrations are generally low (74-3,700 ppm; Table DR1), indicating limited weathering inputs.

The $\delta^{238}U$ values measured from the carbonate fraction almost certainly include U in secondary carbonate cements. If the cements precipitated from oxidizing porewaters (probably in communication with overlying seawater), then the $\delta^{238}U$ value of the cements would be similar to primary seawater precipitates. If the cements precipitated from O_2-poor porewaters that were in partial communication with overlying seawater, then reduction of uranium to U(IV) would have led to preferential fractionation of ^{238}U into the cements, resulting in a positive shift in bulk carbonate $\delta^{238}U$ values relative to the original seawater value (Romaniello et al., 2013). However, fractionation would have been near-zero in a fully closed diagenetic system, in which porewater U was quantitatively taken up by secondary cements. The bulk carbonate fraction likely includes secondary carbonate cements that shifted bulk carbonate $\delta^{238}U$ values in a positive direction relative to the $\delta^{238}U$ of the primary carbonate components (see DR4). We infer that these post-depositional processes affected all of the study samples similarly, shifting them towards higher isotopic values, but that the original marine secular trend is preserved (cf. Romaniello et al., 2013).

In summary, there are no correlations between Th/U or $\delta^{238}U$ and sample $\delta^{18}O$, Mg/Ca, Sr/Ca, or Al compositions that imply alteration of U-system chemistry by siliciclastic inputs, dolomitization, or other diagenetic processes. Hence, we interpret the U concentrations and isotopic compositions of the study samples to represent primary signals of contemporaneous seawater during the F-F transition.

(DR4) MARINE URANIUM CYCLE MODELING

The importance of anoxic facies as a sink for seawater U can be modeled based on the isotopic composition of seawater-sourced U in oxic sediments (e.g., carbonate $\delta^{238}U$; Montoya-Pino et al., 2010; Brennecka et al., 2011; Lau et al., 2016; Elrick et al., 2017). The fraction of U removed to anoxic facies (f_{anox}), and thus the $\delta^{238}U$ of seawater, is controlled mainly by the relative sizes and U-isotopic compositions of the two principal sink fluxes, i.e., oxic/suboxic facies (which also includes any U of hydrothermal origin) and anoxic/euxinic facies:

$$\delta^{238}U_{river} = ((1 - f_{anox}) \times \delta^{238}U_{ox}) + (f_{anox} \times \delta^{238}U_{anox}) \quad \text{(S1)}$$

where ‘river’ is the riverine U-source flux, and ‘ox’ and ‘anox’ represent the oxic/suboxic and anoxic/euxinic sink fluxes, respectively. The fraction of seawater U that is removed to anoxic facies is then calculated as:

$$f_{anox} = (\delta^{238}U_{source} - \delta^{238}U_{ox}) / (\delta^{238}U_{anox} - \delta^{238}U_{ox}) \quad \text{(S2)}$$

where $\delta^{238}U_{anox} = \delta^{238}U_{sw} + \Delta$sw-anox, and $\delta^{238}U_{sw} = \delta^{238}U_{ox} - \Delta$sw-ox (note that Δsw-anox and Δsw-ox are the $\delta^{238}U$ fractionations associated with anoxic/euxinic and oxic/suboxic sinks of seawater uranium, respectively). In principle, isotopically heavier measured carbonate U-isotope compositions (and, hence, $\delta^{238}U_{ox}$ values) indicate a greater importance for oxic/suboxic sinks for seawater U, and isotopically lighter carbonate U-isotope compositions a greater importance for anoxic/euxinic sinks.

All geochemical models make use of simplifying assumptions in order to test various influences in natural systems. The principal assumptions of our steady-state model include (1) a constant U isotopic composition for the riverine source flux, (2) constant fractionation factors between seawater and the oxic/suboxic (Δsw-ox) or anoxic/euxinic sinks (Δsw-anox), and (3) a constant diagenetic correction factor to correct for the influence of ^{238}U-enriched secondary carbonate phases. Whereas the $\delta^{238}U$ composition of modern seawater has been determined fairly accurately, the compositions of modern marine carbonates, continental crustal rocks, and river waters are known only approximately (Weyer et al., 2008; Hiess et al., 2012; Romaniello et al., 2013; Andersen et al., 2014, 2016). More studies will be needed to determine the ranges of isotopic variability in natural U reservoirs and to test the robustness of the assumptions underlying this model. For present purposes, we dealt with these uncertainties by running sensitivity tests in which each of the model parameters was varied

independently to match the observed pattern of $\delta^{238}U_{ox}$ variation (as proxied by the Baisha $\delta^{238}U$ record; Fig. 1D).

Recent studies have helped to characterize the marine uranium cycle. A recent estimate of seawater $\delta^{238}U$ is –0.392(±0.005) ‰ (Tissot and Dauphas, 2015), which is close to the measured values of –0.40 ‰ (e.g., Weyer et al., 2008) and –0.352±0.055 ‰ (Elrick et al., 2017). The $\delta^{238}U$ of the modern riverine flux was reported as –0.27(±0.16) ‰, with a range from –0.72 ‰ to +0.06 ‰ (Andersen et al., 2016). The relatively large variation in modern riverine values speaks to the need for additional studies to clarify the range of typical modern (and ancient) continental $\delta^{238}U$ values. However, this value is close to the average for continental crust, which is –0.29(±0.03) ‰ (Tissot and Dauphas, 2015) as well as for oceanic basalts (Weyer et al., 2008) and the bulk Earth (Goldmann et al., 2015), suggesting little fractionation during weathering and transport of uranium. Metalliferous marine sediments (i.e., deep-ocean Fe-Mn nodules) take up uranium from seawater with a negative fractionation of –0.30 ‰ to –0.20 ‰ (Goto et al., 2014). Primary marine carbonates, on the other hand, take up uranium from oxic waters with little if any fractionation (Δsw-ox ~0‰), as shown in recent laboratory experiments (Chen et al., 2016). Under anoxic conditions, reduction of U(VI) to U(IV) leads preferential uptake of ^{238}U in carbonates, with a fractionation factor (Δsw-anox) that was estimated at +0.5 ‰ by Weyer et al. (2008) but that has been revised to +0.77(±0.04) ‰ based on recent laboratory experiments (Stirling et al., 2015; cf. Elrick et al., 2017).

Our steady-state model algorithms (Eqs. S1-S2) are based on those used in earlier U-isotope studies that modeled paleo-seawater redox variation (e.g., Montoya-Pino et al., 2010; Brennecka et al., 2011), and our parameterization of model variables follows Elrick et al. (2017). We adopted –0.29 ‰ for average riverine $\delta^{238}U$ (based on average crustal $\delta^{238}U$, which is better constrained than actual riverine $\delta^{238}U$) and fractionations of 0 ‰ and +0.77 ‰ for ^{238}U into carbonate sediments under oxic and anoxic conditions, respectively. One additional parameter of our model relevant to analysis of paleo-seawater conditions is the diagenetic correction factor (Δdiag), which is applied to measured (meas) $\delta^{238}U$ values prior to calculation of f_{anox} via Equations S1-S2:

$$\delta^{238}U_{ox} = \delta^{238}U_{meas} + \Delta diag \quad (S3)$$

The application of a diagenetic correction factor is an outgrowth of recent work by Romaniello et al. (2013), who showed that modern marine bulk carbonates at shallow burial depths (<40 cm) yield $\delta^{238}U$ values that are mostly 0.2 ‰ to 0.4 ‰ higher than those of ambient seawater and primary carbonate precipitates at the sediment-water interface. This enrichment of ^{238}U at shallow burial depths was linked to early diagenetic uptake of uranium into secondary carbonate phases (i.e., cements) under reducing conditions (e.g., in the sulfate reduction zone). However, Elrick et al. (2017) showed that values of Δdiag between 0.2 ‰ and 0.4 ‰ resulted in many of their study samples yielding f_{anox} <0 %, and that a larger Δdiag value (0.5 ‰) was necessary to bring the largest proportion of samples within the expected

f_{anox} range of 0-1.0. They suggested that the diagenetic shifts of 0.2 ‰ to 0.4 ‰ reported by Romaniello et al. (2013) do not reflect the final burial stabilization of the sub-Recent carbonates investigated in that study, and that stabilized ancient marine limestones ultimately may record a larger diagenetic shift. In the present study, we found that Δdiag values ranging from 0.3 ‰ to 0.5 ‰ (but not outside this range) yielded f_{anox} estimates between 0 and 1.0 for all study samples. Consequently, we adopted 0.4 ‰ as a median estimate of the Δdiag parameter in this study. We recognize, however, that Δdiag is probably not a constant, and that our study samples are likely to have experienced some variability in early diagenetic U-isotopic shifts.

REFERENCES CITED

Algeo, T.J., 2004, Can marine anoxic events draw down the trace element inventory of seawater?: Geology, v. 32(12), p. 1057-1060.

Alroy, J., 2008. Dynamics of origination and extinction in the marine fossil record: Proceedings of the National Academy of Sciences (U.S.A.), v. 105, p. 11536-11542.

Andersen, M.B., Romaniello, S., Vance, D., Little, S.H., Herdman, R., and Lyons, T.W., 2014, A modern framework for the interpretation of $^{238}U/^{235}U$ in studies of ancient ocean redox: Earth and Planetary Science Letters, v. 400, p. 184-194, doi:10.1016/j.epsl.2014.05.051.

Andersen, M.B., Vance, D., Morford, J.L., Bura-Nakic, E., Breitenbach, S.F.M., and Och, L., 2016, Closing in on the marine $^{238}U/^{235}U$ budget: Chemical Geology, v. 420, p. 11-22, doi:10.1016/j.chemgeo.2015.10.041.

Asael, D., Tissot, F.L., Reinhard, C.T., Rouxel, O., Dauphas, N., Lyons, T.W., Ponzevera, E., Liorzou, C., and Chéron, S., 2013, Coupled molybdenum, iron and uranium stable isotopes as oceanic paleoredox proxies during the Paleoproterozoic Shunga Event: Chemical Geology, v. 362, p. 193-210, doi:10.1016/j.chemgeo.2013.08.003.

Brennecka, G.A., Herrmann, A.D., Algeo, T.J., and Anbar, A.D., 2011, Rapid expansion of oceanic anoxia immediately before the end-Permian mass extinction: Proceedings of the National Academy of Sciences (U.S.A.), v. 108, p. 17631-17634, doi:10.1073/pnas.1106039108.

Chen, D.Z., and Tucker, M.E., 2003, The Frasnian-Famennian mass extinction: insights from high-resolution sequence stratigraphy and cyclostratigraphy in South China: Palaeogeography, Palaeoclimatology, Palaeoecology, v. 193 p. 87-111, doi:10.1016/S0031-0182(02)00716-2.

Chen, D., Tucker, M. E., Jiang, M., and Zhu, J., 2001a, Long-distance correlation between tectonic-controlled, isolated carbonate platforms by cyclostratigraphy and sequence stratigraphy in the Devonian of South China: Sedimentology, v. 48, p. 57-78, doi: 10.1111/j.1365-3091.2001.00351.x.

Chen, D., Tucker, M. E., Zhu, J., and Jiang, M., 2001b, Carbonate sedimentation in a starved pull-apart basin, Middle to Late Devonian, southern Guilin, South China: Basin Research, v. 13, p. 141-167, doi:10.1046/j.1365-2117.2001.00148.x.

Chen, D., Qing, H., and Li, R., 2005, The Late Devonian Frasnian-Famennian (F/F) biotic crisis: Insights from $\delta^{13}C_{carb}$, $\delta^{13}C_{org}$ and $^{87}Sr/^{86}Sr$ isotopic systematics: Earth and Planetary Science Letters, v. 235, p. 151-166.

Chen, X.M, Romaniello, S.J., Herrmann, A.D., Wasylenki, L.E., and Anbar, A.D., 2016, Uranium isotope fractionation during coprecipitation with aragonite and calcite: Geochimica et Cosmochimica Acta, v. 188, p. 189-207, doi:10.1016/j.gca.2016. 05.022.

Chung, G.S., and Swart, P.K., 1990, The concentration of uranium in freshwater vadose and phreatic cements in a Holocene ooid cay: A method of identifying ancient water tables: Journal of Sedimentary Research, v. 60, p. 735-746.

Cumberland, S.A., Douglas, G., Grice, K., and Moreau, J.W., 2016, Uranium mobility in organic matter-rich sediments: A review of geological and geochemical processes: Earth-Science Reviews, v. 159, p. 160-185.

Elrick, M., Polyak, V., Algeo, T.J., Romaniello, S., Asmerom, Y., Herrmann, A.D., Anbar, A.D., Zhao, L., and Chen, Z.Q., 2017, Global-ocean redox variation during the middle-late Permian through Early Triassic based on uranium isotope and Th/U trends of marine carbonates: Geology, v. 45(2), p. 163-166, doi:10.1130/G38585.1.

Goldmann, A., Brennecka, G., Noordmann, J., Weyer, S., and Wadhwa, M., 2015, The uranium isotopic composition of the Earth and the Solar System: Geochimica et Cosmochimica Acta, v. 148, p. 145-158, doi:10.1016/j.gca.2014.09.008.

Goto, K.T., Anbar, A.D., Gordon, G.W., Romaniello, S.J., Shimoda, G., Takaya, Y., Tokumaru, A., Nozaki, T., Suzuki, K., Machida, S., and Hanyu, T., 2014, Uranium isotope systematics of ferromanganese crusts in the Pacific Ocean: Implications for the marine $^{238}U/^{235}U$ isotope system: Geochimica et Cosmochimica Acta, v. 146, p. 43-58, doi:10.1016/j.gca.2014.10.003.

Hiess, J., Condon, D.J., McLean, N., and Noble, S.R., 2012, $^{238}U/^{235}U$ systematics in terrestrial uranium-bearing minerals: Science, v. 335, p. 1610-1614, doi:10.1126/ science.1215507.

Lau, K.V., Maher, K., Altiner, D., Kelley, B.M., Kump, L.R., Lehrmann, D.J., Silva-Tamayo, J.C., Weaver, K.L., Yu, M., and Payne, J.L., 2016, Marine anoxia and delayed Earth system recovery after the end-Permian extinction: Proceedings of the National Academy of Sciences (U.S.A.), v. 113(9), p. 2360-2365, doi:10.1073/pnas. 1515080113.

Ma, X., Gong, Y., Chen, D., Racki, G., Chen, X., and Liao, W., 2016, The Late Devonian Frasnian-Famennian Event in South China–Patterns and causes of extinctions, sea level changes, and isotope variations: Palaeogeography, Palaeoclimatology, Palaeoecology, v. 448, p. 224-244, doi:10.1016/ j.palaeo.2015.10.047.

McLennan, S.M., 2001, Relationships between the trace element composition of sedimentary rocks and upper continental crust: Geochemistry, Geophysics, Geosystems, v. 2(4), paper 2000GC000109, 24 pp.

McManus, J., Berelson, W.M., Klinkhammer, G.P., Hammond, D.E., and Holm, C., 2005, Authigenic uranium: relationship to oxygen penetration depth and organic carbon rain: Geochimica et Cosmochimica Acta, v. 69, p. 95-108, doi:10.1016/j.gca. 2004.06.023.

Montoya-Pino, C., Weyer, S., Anbar, A.D., Pross, J., Oschmann, W., van de Schootbrugge, B., and Arz, H.W., 2010, Global enhancement of ocean anoxia during Oceanic Anoxic Event 2: A quantitative approach using U isotopes: Geology, v. 38, p. 315-318, doi:10. 1130G30652.1.

Morford, J.L., Martin, W.R., and Carney, C.M., 2009, Uranium diagenesis in sediments underlying bottom waters with high oxygen content: Geochimica et Cosmochimica Acta, v. 73, p. 2920-2937, doi:10.1016/j.gca.2009.02.014.

Romaniello, S.J., Herrmann, A.D., and Anbar, A.D., 2013, Uranium concentrations and $\delta^{238}U$ isotope ratios in modern carbonates from the Bahamas: Assessing a novel paleoredox proxy: Chemical Geology, v. 362, p. 305-316, doi:10.1016/j.chemgeo. 2013.10.002.

Sandberg, C.A., Morrow, J.R., and Ziegler, W., 2002, Late Devonian sea-level changes, catastrophic events, and mass extinctions. In: Koeberl, C., and MacLeod, K.G. (Eds.), Catastrophic Events and Mass Extinctions: Impacts and Beyond: Geological Society of America Special Paper 356, pp. 473-487, doi:10.1130/0-8137-2356-6.473.

Shen, J.W., and Webb, G.E., 2004, Famennian (Upper Devonian) calcimicrobial (Renalcis) reef at Miaomen, Guilin, Guangxi, South China. Palaeogeography, Palaeoclimatology, Palaeoecology, v. 204(3), p. 373-394, doi:10.1016/S0031-0182(03)00737-5.

Spalletta, C., Perri, M.C., Over, D.J., and Corradini, C., 2017, Famennian (Upper Devonian) conodont zonation: revised global standard: Bulletin of Geosciences, v. 92(1), p. 31-57.

Stigall, A.L., 2012, Speciation collapse and invasive species dynamics during the Late Devonian "Mass Extinction": GSA Today, v. 22(1), p. 4-9.

Stirling, C.H., Andersen, M.B., Warthmann, R., and Halliday, A.N., 2015, Isotope fractionation of ^{238}U and ^{235}U during biologically-mediated uranium reduction: Geochimica et Cosmochimica Acta, v. 163, p. 200-218, doi:10.1016/j.gca.2015.03.017.

Thomson, J., Jarvis, I., Green, D.R., Green, D.A., and Clayton, T., 1998, Mobility and immobility of redox-sensitive elements in deep-sea turbidites during shallow burial: Geochimica et Cosmochimica Acta, v. 62(4), p. 643-656.

Tissot, F.L., and Dauphas, N., 2015, Uranium isotopic compositions of the crust and ocean: Age corrections, U budget and global extent of modern anoxia: Geochimica et Cosmochimica Acta, v. 167, p. 113-143, doi:10.1016/j.gca.2015.06.034.

Wang, C.Y., and Ziegler, W., 2002, The Frasnian-Famennian conodont mass extinction and recovery in south China. Palaeobiodiversity and Palaeoenvironments, v. 82(2), p. 463-493, doi:10.1007/BF03042948.

Weyer, S., Anbar, A.D., Gerdes, A., Gordon, G.W., Algeo, T.J., and Boyle, E.A., 2008, Natural fractionation of $^{238}U/^{235}U$: Geochimica et Cosmochimica Acta, v. 72(2), p. 345-359, doi:10.1016/j.gca.2007.11.012.

Wignall, P.B., and Twitchett, R.J., 1996, Oceanic anoxia and the end Permian mass extinction: Science, v. 272, p. 1155-1158, doi:10.1126/science.272.5265.1155.

Ziegler, W., and Sandberg, C.A., 1990, The Late Devonian standard conodont zonation: Courier Forschungsinstitut Senckenberg, v. 121, 115 pp.

SUPPLEMENTARY TABLES AND FIGURES

Table DR1. Geochemical data from Baisha section

Sample No	Strat. Elev. (m)	TOC (%)	$\delta^{13}C$ (‰)	$\delta^{18}O$ (‰)	$\delta^{238}U$ (‰)	Mg/Ca	Sr/Ca ($x10^{-4}$)	Al (ppm)	Th/U	Th (ppm)
BS-1	0.05	0.14	0.23	-5.88	-0.32	0.01	6.06	224	0.46	0.32
BS-5	0.85	0.12			-0.37	0.01	6.96	206	0.93	0.09
BS-2	1.65	0.13	0.92	-4.95	-0.41	0.02	5.54	142	0.65	0.20
BS-3	3.15	0.53	2.63	-6.11	-0.18	0.01	5.26	291	0.56	0.34
BS-4	5.35	0.44	3.01	-5.85	-0.22	0.01	4.88	283	0.22	0.24
BS-6	8.55	0.10	1.21	-6.47		0.01	4.35	74	0.19	0.09
BS-7	9.55	0.11	1.53	-5.88	-0.21	0.01	6.01	82	0.25	0.20
BS-8	11.55	0.12	0.81	-6.67	-0.12	0.01	5.98	350	0.54	0.47
BS-9	14.05	0.09	0.71	-6.76	-0.20	0.01	3.84	1403	4.54	1.10
BS-10	15.55	0.09	0.70	-6.64		0.02	5.02	2727	6.60	1.74
BS-11	17.55	0.13	0.53	-5.86	-0.15	0.01	6.36	2117	2.18	1.08
BS-12	19.55	0.10	0.57	-6.72	-0.42	0.01	4.14	2830	16.14	2.01
BS-13	21.05	0.12	0.13	-6.37	-0.54	0.03	6.81	2332	8.64	3.15
BS-14	23.05	0.23	2.34	-6.66	-0.38	0.01	6.77	630	2.01	0.50
BS-15	25.05	0.13	3.58	-6.29	-0.29	0.01	5.60	2225	3.12	1.42
BS-16	27.05	0.10	2.79	-6.66	-0.25	0.02	3.81	3765	22.94	2.48
BS-17	29.05	0.09	2.22	-6.10	-0.18	0.01	4.57	2712	3.84	1.50
BS-18	31.05	0.09	2.01	-6.63	-0.21	0.04	4.56	2885	9.41	1.58
BS-19	33.05	0.10	1.73	-6.77	-0.49	0.03	5.15	3718	23.33	2.72
BS-20	35.05	0.12	1.57	-5.72	-0.33	0.01	5.56	782	1.35	0.60
BS-21	37.05	0.12	1.73	-5.44	-0.33	0.01	6.27	754	0.91	0.54
BS-22	39.05	0.12	1.96	-5.32	0.00	0.01	5.96	326	1.02	0.33
BS-23	41.05	0.09	2.26	-6.45	-0.23	0.01	4.15	1554	8.86	1.07
BS-24	43.05	0.09	1.73	-5.86	-0.16	0.01	4.29	658	1.68	0.56
BS-25	45.05	0.10	1.65	-5.85	-0.24	0.01	3.69	380	0.84	0.27
BS-26	47.05	0.10	1.72	-5.96	-0.25	0.01	4.20	1933	5.78	1.18

387

388

389 Table DR2. Modeling results of fractional anoxic sink flux [$f_{(anox)}$] and seafloor anoxic area

390

Sample No	Strat. Elev. (m)	$\delta^{238}U$ (‰) raw	$\delta^{238}U$ (‰) corrected†	$f_{(anox)}$	$f_{(ox)}$	Seafloor anoxic area (%)	U_{conc} (nM)
BS-1	0.05	-0.32	-0.72	0.56	0.44	5	1.93
BS-5	0.85	-0.37	-0.77	0.62	0.38	7	1.67
BS-2	1.65	-0.41	-0.81	0.68	0.32	9	1.45
BS-3	3.15	-0.18	-0.58	0.38	0.62	3	2.65
BS-4	5.35	-0.22	-0.62	0.43	0.57	3	2.43
BS-6	8.55						
BS-7	9.55	-0.21	-0.61	0.42	0.58	3	2.48
BS-8	11.55	-0.12	-0.52	0.29	0.71	2	2.98
BS-9	14.05	-0.20	-0.60	0.40	0.60	3	2.57
BS-10	15.55						
BS-11	17.55	-0.15	-0.55	0.34	0.66	2	2.80
BS-12	19.55	-0.42	-0.82	0.68	0.32	9	1.43
BS-13	21.05	-0.54	-0.94	0.84	0.16	19	0.80
BS-14	23.05	-0.38	-0.78	0.64	0.36	7	1.61
BS-15	25.05	-0.29	-0.69	0.52	0.48	5	2.08
BS-16	27.05	-0.25	-0.65	0.47	0.53	4	2.29
BS-17	29.05	-0.18	-0.58	0.38	0.62	3	2.66
BS-18	31.05	-0.21	-0.61	0.42	0.58	3	2.50
BS-19	33.05	-0.49	-0.89	0.78	0.22	13	1.07
BS-20	35.05	-0.33	-0.73	0.57	0.43	5	1.90
BS-21	37.05	-0.33	-0.73	0.57	0.43	6	1.89
BS-22	39.05	0.00	-0.40	0.14	0.86	1	3.58
BS-23	41.05	-0.23	-0.63	0.44	0.56	3	2.38
BS-24	43.05	-0.16	-0.56	0.35	0.65	2	2.75
BS-25	45.05	-0.24	-0.64	0.45	0.55	3	2.37
BS-26	47.05	-0.25	-0.65	0.47	0.53	4	2.30

†Corrected for 0.4 ‰ diagenetic shift in primary marine carbonate $\delta^{238}U$.

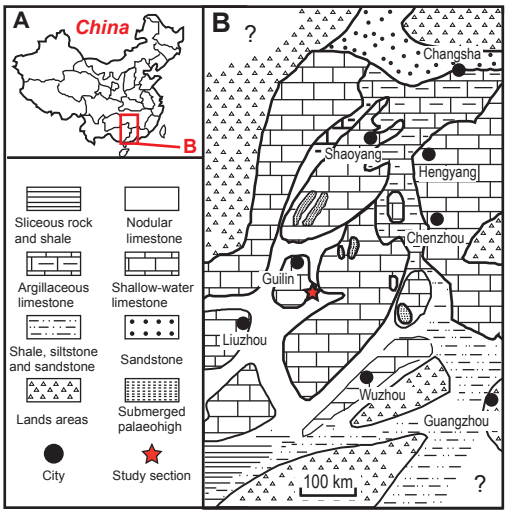
A
China
B
B
?
Changsha
Shaoyang
Hengyang
Chenzhou
Guilin
Liuzhou
Wuzhou
Guangzhou
100 km
?
Sliceous rock and shale
Nodular limestone
Argillaceous limestone
Shallow-water limestone
Shale, siltstone and sandstone
Sandstone
Lands areas
Submerged palaeohigh
City
Study section

Figure DR1

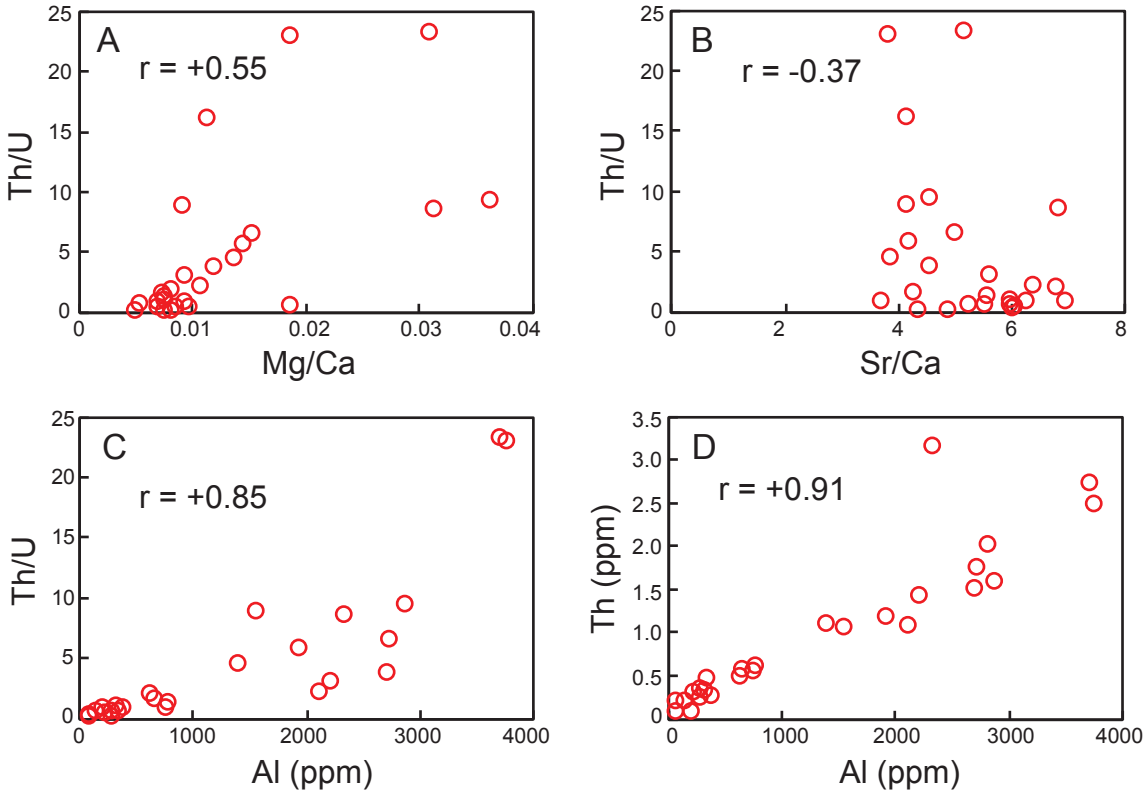
A
r = +0.55
Th/U
Mg/Ca
B
r = -0.37
Th/U
Sr/Ca
C
r = +0.85
Th/U
Al (ppm)
D
r = +0.91
Th (ppm)
Al (ppm)

Figure DR2

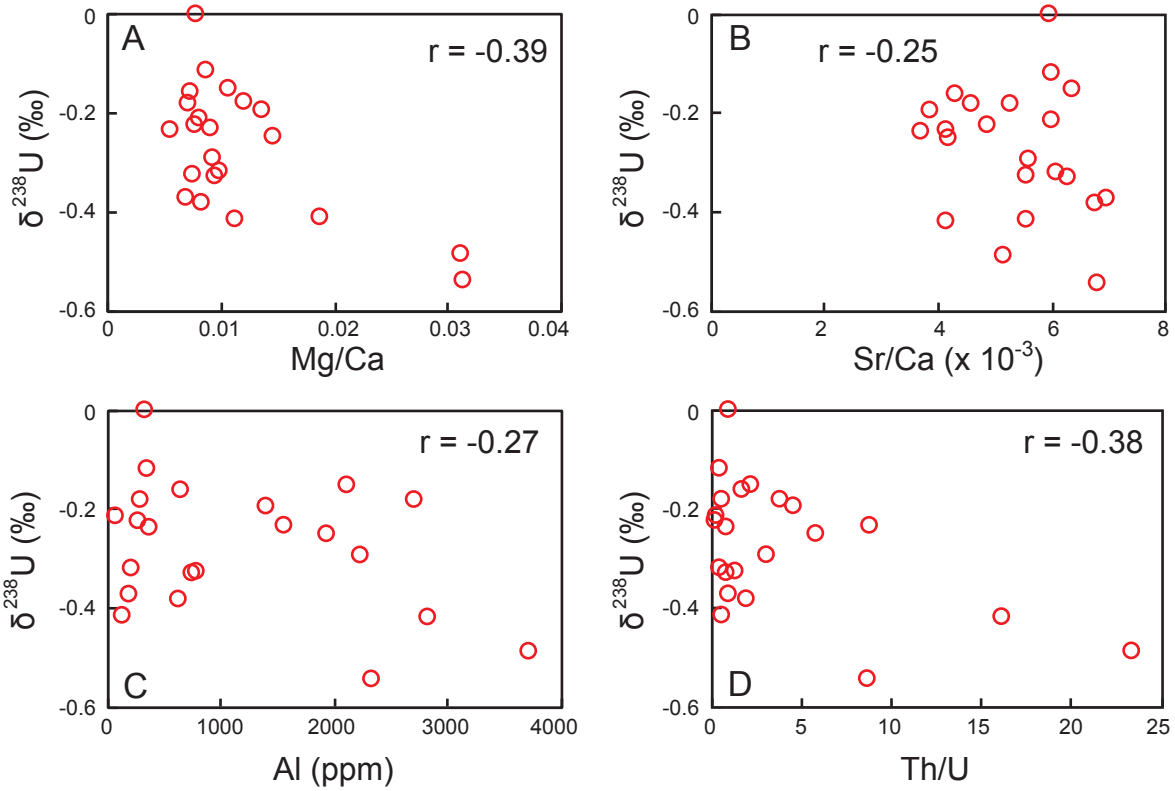

Figure DR3

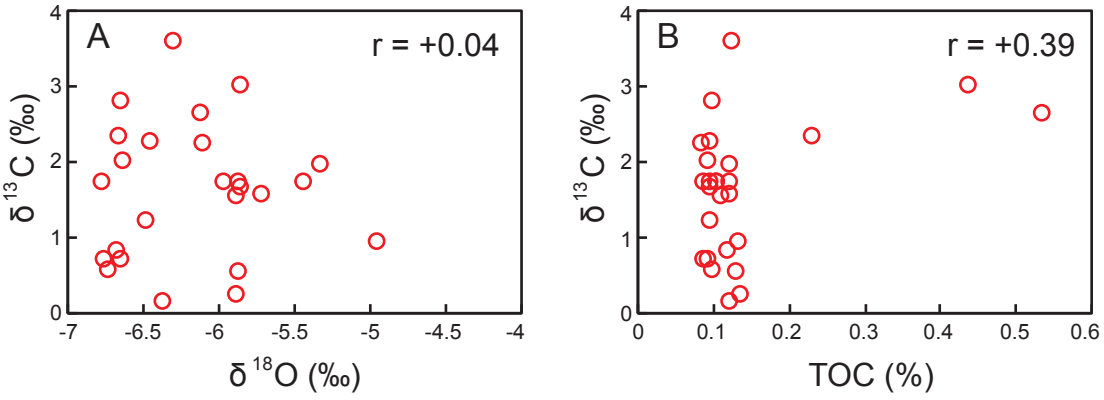

Figure DR4